



Imaging CdCl₂ defect passivation and formation in polycrystalline CdTe films by cathodoluminescence

Thomas Bidaud ¹, John Moseley,² Mahisha Amarasinghe,^{2,3} Mowafak Al-Jassim,² Wyatt K. Metzger,² and Stéphane Collin ^{1,*}

¹Centre de Nanosciences et de Nanotechnologies, CNRS, Université Paris-Saclay, 91120 Palaiseau, France

²National Renewable Energy Laboratory, Golden, Colorado 80401, USA

³University of Illinois at Chicago, Chicago, Illinois 60607, USA



(Received 7 December 2020; accepted 19 May 2021; published 3 June 2021)

Polycrystalline thin-film solar cells are attractive for low-cost photovoltaics, but their efficiencies are hindered by material quality issues. State-of-the-art CdTe solar cells use CdCl₂ annealing treatments whose effects are still being discovered at a fundamental level. Here, a series of CdTe samples with different annealing temperatures is investigated with high-resolution hyperspectral cathodoluminescence mapping measured at both room temperature and low temperature on the same microscopic areas. A statistical analysis over a large number of grains is combined with a local analysis at grain boundaries. The results elucidate the dynamic interplay between grain boundary and intragrain defect passivation and formation, in the midst of grain growth. The CdCl₂ annealing initially contributes to an increase of the grain size and the passivation of both grain boundaries and grain interiors, increasing the overall luminescence and diffusion length. For higher annealing temperatures, a further increase of grain size is counterbalanced by the rise of bulk defects. The results illustrate the tradeoffs that lead to an optimal annealing temperature, as well as new methods for understanding defect passivation and creation in thin film solar cells.

DOI: [10.1103/PhysRevMaterials.5.064601](https://doi.org/10.1103/PhysRevMaterials.5.064601)

I. INTRODUCTION

Polycrystalline thin films based on Cu(In,Ga)(S,Se)₂ (CIGS) and CdTe are attractive options for low-cost photovoltaics [1]. These films only need to be a few microns thick due to high absorption coefficients, and they can be deposited rapidly, enabling high-throughput manufacturing. However, thin-film solar cell efficiencies have yet to reach levels (relative to theoretical limits) achieved by monocrystalline solar cells based on silicon or GaAs. Limitations are ascribed to the very nature of polycrystalline thin films: the limited grain size, the detrimental role of grain boundaries, bulk defects, and difficulty controlling carrier concentration [2–5]. The development of postdeposition treatments has enabled tremendous improvements in the material quality and doping levels [6–10]. These treatments involve annealing in the presence of extrinsic elements such as alkali in the case of CIGS, and chlorine for CdTe, for instance. Annealing of CdTe thin films in CdCl₂ atmosphere provides an essential boost to CdTe device efficiency [11–15]. While much is known about CdCl₂'s transformative effects, e.g., recrystallization, grain growth, and grain boundary passivation [12,16–19], much can still be learned at a more fundamental level.

Grain boundaries (GBs) are highly defective regions that can enhance nonradiative recombination and reduce the power-conversion efficiency of polycrystalline solar cells. Cathodoluminescence (CL) contrast data on CdTe thin

films indicate GB recombination velocities on the order of 10⁵–10⁶ cm s⁻¹ [2,20]. Kelvin probe force microscopy [21], electron-beam-induced current [22–24], and other microscopic measurements [25] have shown that GBs can develop electrostatic potentials on the order of 50–100 mV that attract and channel minority carriers to the *pn* junction. According to numerical simulations, these potentials can provide a small increase in current collection, but they also increase recombination in forward bias and reduce the open-circuit voltage (V_{oc}). The overall tradeoff for efficiency is predicted to be negative for GB recombination velocity and potential values that are consistent with measurements [26].

The grain size is a critical parameter determining the magnitude of GB performance impacts. For example, the V_{oc} is predicted to vary as the natural logarithm of the grain size (assuming columnar grains that are not fully depleted) [14,27]. The potential to improve V_{oc} through increasing grain size was demonstrated by monocrystalline CdTe solar cells [4,25,28]. These cells achieved $V_{oc} > 1$ V, which is substantially above the highest reported value for polycrystalline cells [29,30]. Unfortunately, the epitaxial and bulk-crystal growth methods used for these monocrystalline cells are not compatible with high-throughput manufacturing.

Variations of typical thin film processing—that are manufacturing-compatible—have produced films with relatively large grains. These include (i) increasing the O₂ partial pressure during CdTe deposition [7,31], and (ii) increasing the temperature or duration of the postdeposition CdCl₂ annealing step [14,15,32]. To date, both of these strategies found V_{oc} peaks that did not coincide with the maximum grain size

*stephane.collin@c2n.upsaclay.fr

[13,14]. These results indicate that there are other factors besides GB recombination, such as grain interior (GI) or interface defects, that limit performances in large-grain films produced by these strategies. For instance, an optimal CdCl₂ annealing temperature around 390–430 °C is used in state-of-the-art polycrystalline CdTe and CdSeTe solar cells [14,32–34].

In this work, we use cathodoluminescence (CL) spectrum imaging to study CdTe thin films for a range of CdCl₂ annealing temperatures and grain sizes. We collect room- and low-temperature CL maps on the very same microscopic areas of samples annealed under different CdCl₂ temperatures (400, 420, 440, and 460 °C) and as-deposited. By combining local and statistical analyses, we describe the impact of the annealing temperature on the passivation and formation of defects at the grain boundaries and in the grain interiors. Our results highlight the importance of GI defects to realizing the performance gains possible with larger grains.

II. EXPERIMENTAL DETAILS

A. Sample preparation

Superstrate solar cells with the structure glass/SnO₂:F/Mg_xZn_{1-x}O/CdTe were fabricated. 100-nm-thick Mg_xZn_{1-x}O films were deposited on SnO₂:F-coated soda-lime glass (commercial TEC 12D) by radiofrequency magnetron sputtering using a mixed-oxide target with composition 11 wt.% MgO/89 wt.% ZnO. CdTe layers were grown to thicknesses of 4–5 μm by close-spaced sublimation (CSS) using 600 °C substrate/660 °C source temperatures in a 20% O₂ ambient. CdCl₂ annealing treatments were performed by CSS over a range of CdCl₂ source temperatures: 400–460 °C. CdTe surfaces were flattened for CL by glancing angle Ar⁺-ion milling using 3 kV voltage in a JEOL Cross-Section polisher tool.

B. Cathodoluminescence

CL measurements were performed in an Attolight Chronos CL-scanning electron microscope (SEM) system. Luminescence was collected by an achromatic reflective objective (numerical aperture 0.72) that provides constant collection efficiency over a field of view of about 150 μm in diameter. The acceleration voltage of the electron beam was set to 6 kV, and the current of 2 nA was kept constant within less than 5%. The constant excitation and collection efficiencies during the whole experiments allowed for a quantitative comparison of the luminescence emitted from the different samples. At 6 keV, CASINO simulation shows that 75% and 95% of carriers are generated in a pear-shaped excitation volume within a radius of approximately 25 and 75 nm, respectively. Luminescence spectra were dispersed with a Horiba diffraction grating (150 grooves/mm) and recorded with an Andor Newton charge-coupled-device (CCD) camera (1024 × 256 pixels, pixel width 26 μm). The corresponding spectral dispersion was 0.53 nm per pixel. Luminescence spectra were corrected for the diffraction efficiency of the grating and the sensitivity of the CCD camera. The luminescence intensity described in the text corresponds to a spectral density of photon flux per unit of energy (counts s⁻¹ eV⁻¹).

III. RESULTS AND DISCUSSION

A. Room-temperature CL maps

The panchromatic CL maps measured at room temperature on the five samples are plotted in Figs. 1(a)–1(e) using a common linear intensity scale. The polycrystalline nature of the CdTe thin films is clear. Low-intensity (dark) regions correspond to grain boundaries (GBs) [35], where nonradiative recombination is enhanced (due to high misorientation between grains and dangling bonds) [36,37]. Grain interiors (GIs) appear as brighter areas.

For the as-deposited CdTe [Fig. 1(a)], the CL map shows small grains with an average equivalent diameter of ~1.2 μm. This sample also exhibits very inhomogeneous CL intensities, with stronger emission from larger grains. For CdCl₂ treated films, the average grain size increases from 1.4 to 3.2 μm for CdCl₂ anneals ranging from 400 °C [Fig. 1(b)] to 460 °C [Fig. 1(e)]. This progression correlates with an improved CL homogeneity. Interestingly, the highest CL intensity is observed for an annealing temperature of 420 °C, rather than the larger grains obtained at 460 °C.

A statistical analysis of the CL intensities measured on each map is presented in Figs. 1(f)–1(j). The histograms (in gray) show the pixel counts as a function of the luminescence intensity. Interestingly, they exhibit two distinct families, which we identify as GBs (low-intensity peak) and GIs (high-intensity peak). In Figs. 1(f)–1(h), the histograms are accurately fit with the sum of 2-Gaussian functions (red curves) defined by the mean intensities (I_{GI} and I_{GB}), standard deviations (σ_{GI} and σ_{GB}), and amplitudes (N_{GI} and N_{GB}). In Figs. 1(i) and 1(j), the GI peaks are much narrower and the two families no longer overlap. The upper and lower parts of the histograms are fit separately by 1-Gaussian functions, allowing for a third family with intermediate intensities. The fit parameters are given in Table I. They provide a convenient way to assess quantitatively the impact of the CdCl₂ annealing on the CdTe luminescence properties.

The evolution of the mean CL intensities I_{GI} and I_{GB} is shown in Fig. 2. The intensity I_{GB} increases with the annealing temperature up to 420 °C, indicating a partial passivation of the nonradiative grain boundary defects [2,20]. Notably, no further improvement of I_{GB} is seen for temperatures above 420 °C. This passivation is likely due to the diffusion and accumulation of chlorine atoms at the grain boundaries, as observed by TOF-SIMS after CdCl₂ annealing at similar temperatures [38,39]. Segregation of Cl at grain boundaries has also been evidenced by STEM [40]. According to density functional theory (DFT) simulation, substitution of Te by Cl (Cl_{Te}) is energetically favored in a very narrow region around the GB. It may passivate interfacial states [36] and result in a charge accumulation [40]. Cl atoms can also diffuse deeper into the grain interiors [38,41]. The deep-level defects due to cadmium vacancies (V_{Cd}) may be replaced by (Cl_{Te}- V_{Cd}) complexes that act as shallow acceptors [38,42]. Low-temperature CL experiments shown in Sec. III B will provide more insight into the dynamics of shallow defects during the CdCl₂ annealing.

The same trend is found for I_{GI} , with the brightest grains observed at 420 °C. For higher annealing temperatures, the luminescence is more homogeneous in the GIs [Figs. 1(d) and

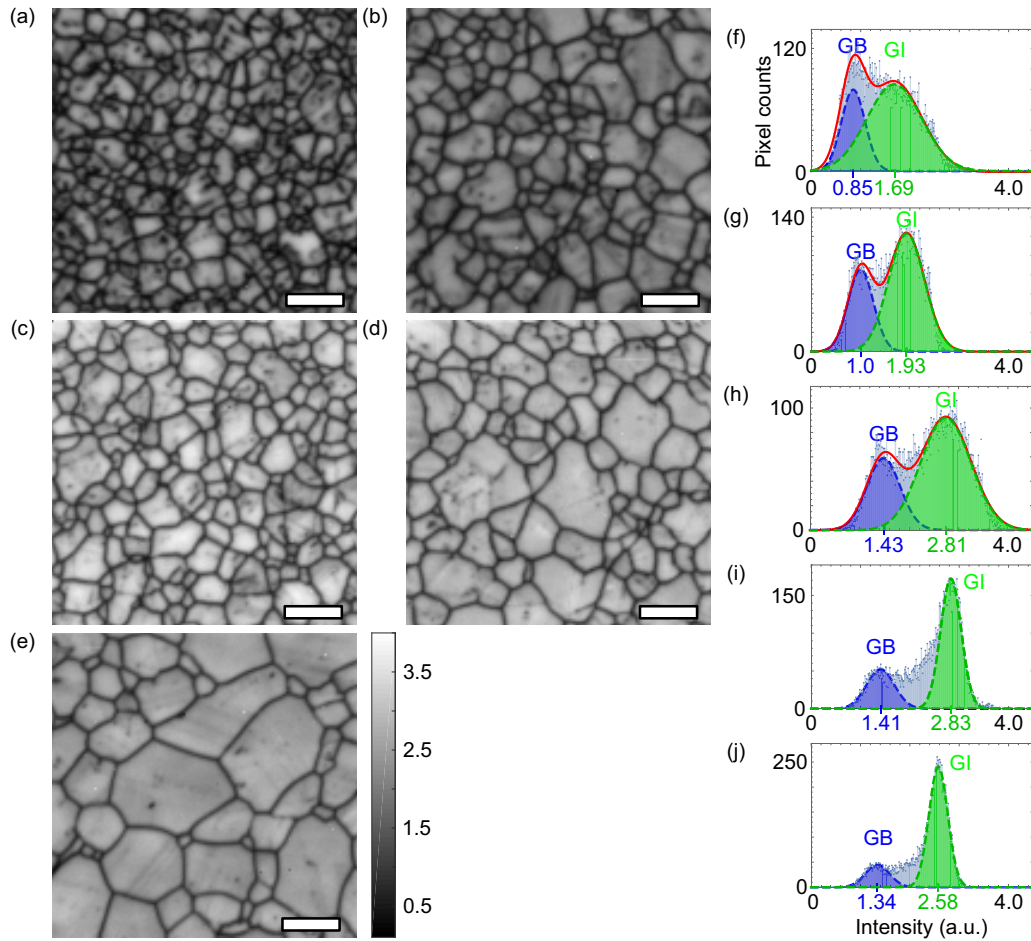


FIG. 1. Panchromatic CL maps (128×128 pixels) of CdTe samples with different CdCl₂ annealing treatments: (a) as-deposited, (b) 400 °C, (c) 420 °C, (d) 440 °C, and (e) 460 °C. All images have been normalized on the same gray scale (scale bar: 5 μm). On the right, room-temperature intensity histograms for each sample with a 2-Gaussian function fit for (f) as-deposited, (g) 400 °C, (h) 420 °C, (i) 440 °C, and (j) 460 °C CdCl₂ treatments.

1(e)], which correlates with narrower intensity distributions [Figs. 1(i) and 1(j)] and a slight decrease in I_{GI} . The behavior is related to the appearance of regions with intermediate luminescence intensity. In the Appendix, the CL maps are plotted with false colors to show the spatial distribution of each family: low intensity at GBs (blue), high intensity in the GIs (green), and intermediate intensity (red). For the higher annealing temperatures (440 and 460 °C), this third family

emerges in grain interiors. Overall, these results are consistent with a decrease in the defect density in grain interiors for annealing temperatures up to 420 °C and the appearance of new defective regions for higher temperatures.

The decrease of the CL intensity close to GBs provides insight into the impact of the defect densities on carrier diffusion lengths. This analysis was performed with another series of CL maps recorded in other areas of the same samples

TABLE I. Fitting parameters of each family of pixels (grain boundary and grain interior) using two Gaussian functions; see Fig. 1. The values are normalized to the mean value of I_{GB} obtained for the sample annealed at 400 °C. An average grain area is determined for each sample, and expressed using the grain diameter of a circle of the same area. The average characteristic length (L_{charac}) is determined by fitting the luminescence decay close to grain boundaries with Eq. (1); see Fig. 3.

Sample	Mean value I_{GB}	Standard deviation σ_{GB}	Mean value I_{GI}	Standard deviation σ_{GI}	Grain diameter (μm)	Characteristic length (μm)
As-deposited	0.85	0.24	1.69	0.56	1.45(0.39)	0.24
400 °C	1.00	0.26	1.93	0.56	1.74(0.5)	0.27
420 °C	1.43	0.27	2.81	0.42	1.77(0.47)	0.34
440 °C	1.41	0.28	2.83	0.21	1.9(0.58)	0.29
460 °C	1.34	0.25	2.58	0.19	3.19(0.84)	0.22

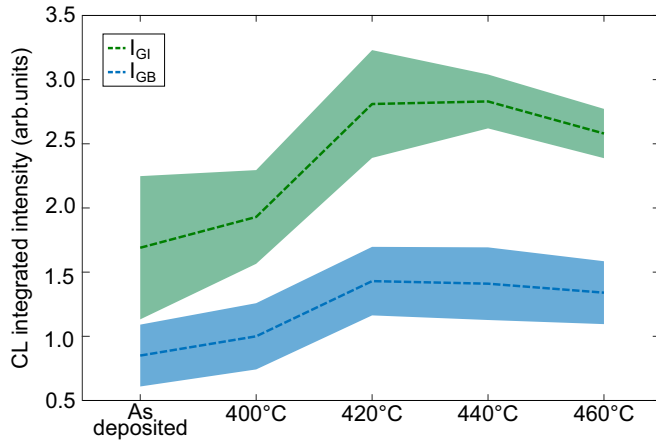


FIG. 2. Plot of the evolution of the I_{GI} and I_{GB} intensity values as a function of the CdCl_2 annealing temperature. The colored areas show the standard deviations (σ_{GI} , σ_{GB}) of the Gaussian distributions fitted in Figs. 1(f)–1(j) for both GI and GB pixel families.

but with a higher spatial resolution (256×256 pixels over $30 \mu\text{m} \times 30 \mu\text{m}$). They allow a more accurate investigation of the diffusion lengths. Figure 3(a) shows a detailed region of a CL map and a CL profile around a GB [Fig. 3(b)]. It can be fit with a simple one-dimensional diffusion model [43–46] describing the decay of the luminescence intensity from the grain interior ($x_{GI} > 0$) toward the grain boundary ($x = 0$). The model considers a characteristic length L_{charac} and a reduced surface recombination velocity S at the grain boundary ($S = s \times \tau / L_{\text{charac}}$, with s the recombination velocity at GB

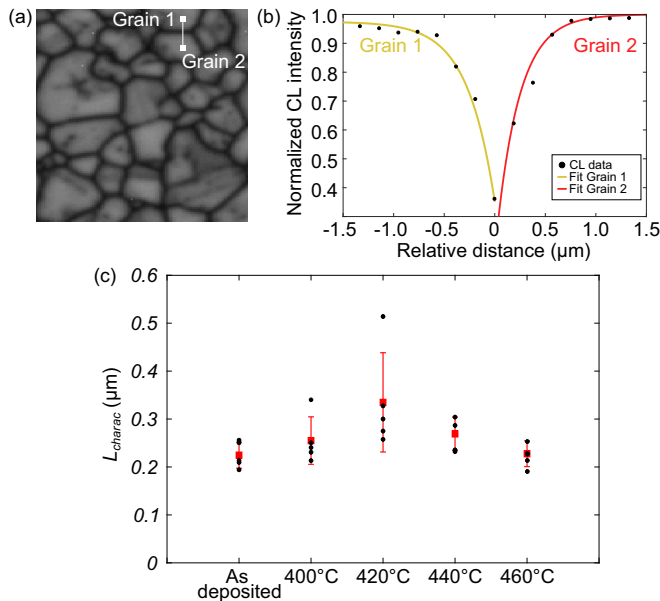


FIG. 3. [(a),(b)] Sample annealed under CdCl_2 at 400°C : panchromatic CL map of a close view (a), and line-scan example of the CL intensity through a GB (b). The CL intensity profile (black dots) is fitted with exponential functions [Eq. (1), red and orange curves]. (c) Characteristic lengths (L_{charac}) determined across five different grain boundaries (black dots) for each sample, and mean values and standard deviations (red).

and τ the intragrain lifetime):

$$\ln\left(1 - \frac{I(x)}{I(x_{GI})}\right) = \frac{S}{S+1} - \frac{x}{L_{\text{charac}}}. \quad (1)$$

L_{charac} equals the diffusion length if recombination at the top and bottom surfaces is negligible. Equation (1) is used to fit the decay of the luminescence close to GBs; see Fig. 3(b). The results obtained for the full set of samples are shown in Fig. 3(c). L_{charac} is found to increase with the annealing temperature up to 420°C and to decrease for higher temperature. This is consistent with the evolution of the grain interior intensity I_{GI} . The larger standard deviation obtained for 420°C reflects the heterogeneous CL intensity between grains observed in Fig. 1. The longer L_{charac} correspond to brighter grains, with values above $0.6 \mu\text{m}$.

In summary, room-temperature panchromatic CL maps show the positive effect of the annealing for temperatures up to 420°C , with a partial passivation of grain boundary defects (increased CL intensity I_{GB}) and an improvement of the radiative efficiency in grain interiors (I_{GI}). At higher temperatures, the detrimental impact of the annealing under CdCl_2 is observed with the decreased luminescence I_{GI} and a lower L_{charac} , which may be due to an increased density of defects in grain interiors.

B. Low-temperature CL maps

To gain insight into the role of defects on both the luminescence and characteristic length, we have collected low-temperature (LT) CL maps (holder temperature 10 K) on the same areas as the room-temperature maps. We first present results for the as-deposited sample in Fig. 4. The CL spectrum averaged over the full 128×128 pixels area is plotted in Fig. 4(a). Three spectral bands are clearly identified: the excitonic band with a peak at 1.596 eV [47], and two defect bands at lower energies. The low-energy band around $1.25\text{--}1.4 \text{ eV}$ is the Z-band defect ascribed to donor-acceptor pair recombination between shallow donors and deep acceptors (V_{Cd} vacancies) [48]. The band at $1.45\text{--}1.5 \text{ eV}$ is attributed to A-center defects induced by complexes formed between V_{Cd} and shallow donors [9,42,47]. The presence of A-centers on the as-deposited sample may be explained by the presence of impurities such as O or Cu. These defect bands have been widely studied in low-temperature photoluminescence experiments [9,42,46–48].

Here, we investigate their spatial distribution over a large number of grains with high resolution, as shown in Fig. 4(b). False colors are attributed to the three spectral bands, and the color indicates the predominant recombination process, either through the excitonic transition (green) or a defect level (red and blue). Interestingly, A- and Z-bands are found in different grains with no or very little overlap. This is consistent with the origin of these defects related to cadmium vacancies alone (Z-band), or that form complexes with shallow donors (A-band). Only one of the two luminescence bands is observed in each grain, and in most grains, the predominant emission is uniformly distributed in the grain interior.

What is the effect of thermal processes on these defects? Annealing CdTe thin films in a CdCl_2 ambient is well known to strongly improve solar cell performance through a decrease

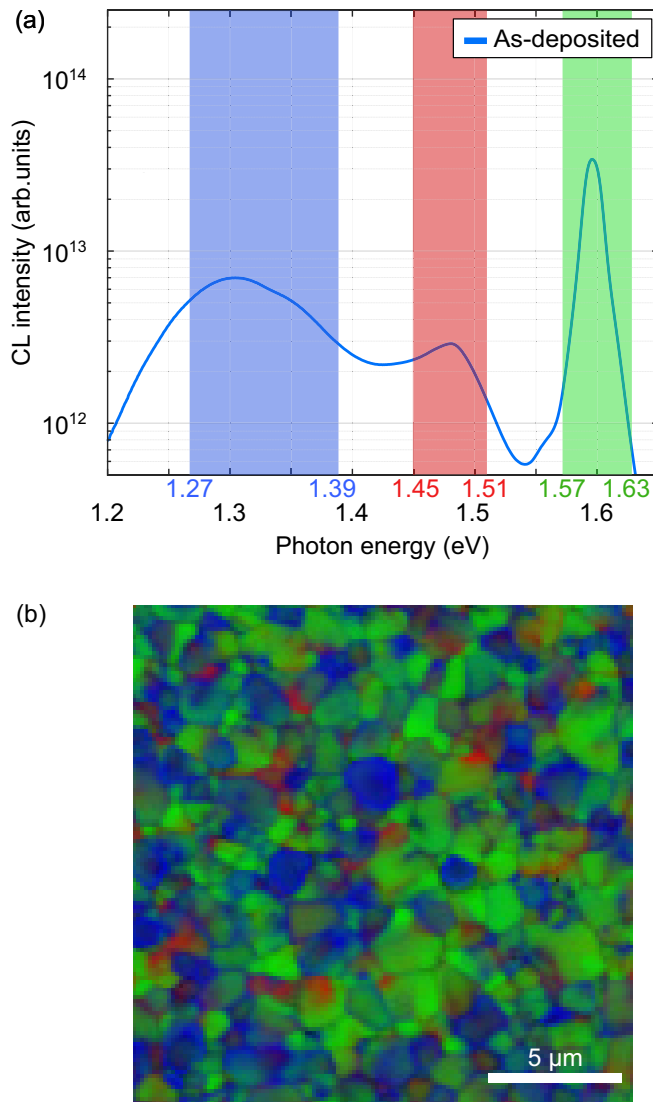


FIG. 4. (a) Low-temperature (10 K) average CL spectrum (128×128 pixels) for the as-deposited sample. (b) Low-temperature CL map with false colors showing the luminescence integrated over three different spectral regions: blue [1.27 eV, 1.39 eV], red [1.45 eV, 1.51 eV], and green [1.57 eV, 1.63 eV]. For each pixel, the integrated intensity of each band is normalized by the intensity integrated over the full spectral range. Scale bar: $5 \mu\text{m}$.

of nonradiative recombination. However, the evolution of the defect bands upon annealing and the mechanisms that lead to an optimal temperature are not fully understood. In the following, we study the impact of the annealing at different temperatures on the nature, density, and spatial distribution of the defects.

CL maps have been measured at low temperature over the very same area as previous RT maps, and they are compared in Fig. 5. This allows a direct comparison between the radiative properties and characteristic lengths investigated at room temperature with the defects revealed by low-temperature measurements. The LT CL spectra averaged over the whole maps are shown in Fig. 5(a) for the different annealing temperatures, T . Contrary to the as-deposited thin film, they exhibit

a single defect band in the 1.35–1.5 eV spectral range. The disappearance of the Z-band can be attributed to the passivation effect of the V_{Cd} by the Cl introduced during the CdCl₂ treatment.

The intensity of each emission band varies with the annealing temperature. The luminescence of the excitonic band increases monotonically with T , with a slight redshift of the peak energy, as shown in Figs. 5(a) and 5(b). On the contrary, we observe a decrease of the emission through the defect band by a factor of more than 2 when T is increased from 400 to 420 °C. The spatial distribution of these defects is shown in Figs. 5(k) and 5(l), respectively. At $T = 400$ °C, the defect density seems to be homogeneous within each grain, and we observe strong variations from one grain to another with no obvious correlation with the grain size. At $T = 420$ °C, the emission is strongly reduced and is much more homogeneous [see Fig. 5(l)]. This is consistent with the higher luminescence in the room-temperature measurements, Fig. 5(d).

For annealing at higher temperatures, the LT CL maps clearly reveal an increase in the defect density [see Figs. 5(m) and 5(n) and the integrated CL intensity in Fig. 5(b)]. We observe a higher luminescence of the defect band in the grain interiors, in particular in larger grains. This phenomenon is consistent with the diffusion of more Cl into grain interiors at the higher annealing temperatures, forming Cl_{T_e} defects. Cl concentrations of $(1 - 5) \times 10^{16} \text{ cm}^{-3}$ have been found in the grain interiors for similar CdCl₂ annealing processes [9,38]. As explained above, at low concentration Cl_{T_e} form complexes with V_{Cd} and thereby eliminate deep levels. Interestingly, our results suggest that above a certain threshold, Cl may form isolated Cl_{T_e} defects that contribute to an increase of the LT A-band emission with a detrimental effect on RT luminescence in the GI. We also note a change of the width and shape of the A-band for different temperatures, which may conceal different defect contributions.

For the highest annealing temperature of $T = 460$ °C, the growth of large grains results in more visible structural defects due to twin boundaries (lines) and dislocations (dark dots). They are evidenced by gray regions in the LT CL maps [Figs. 5(j) and 5(n)], which can be distinguished from grain boundaries with lower luminescence. These structural defects are also responsible for regions with lower luminescence at room temperature [35], as observed in Figs. 5(f) and 6 [red regions in grain interiors corresponding to the intermediate family of pixels in Figs. 5(d) and 5(e)]. These structural defects do not contribute significantly to the A-band emission and do not explain the higher defect concentration in grain interiors for temperatures above 420 °C.

IV. CONCLUSION

We presented high-resolution cathodoluminescence maps measured at both room temperature and low temperature on the same microscopic area for as-deposited samples and samples annealed at different temperatures. For temperatures up to 420 °C, we have shown that the CdCl₂ annealing contributes to the passivation of both GB and GI defects. This correlates with an increase of the grain size, of the GI diffusion lengths, and of the overall luminescence. Beyond 420 °C, the grain size continues to increase without additional passivation of GBs.

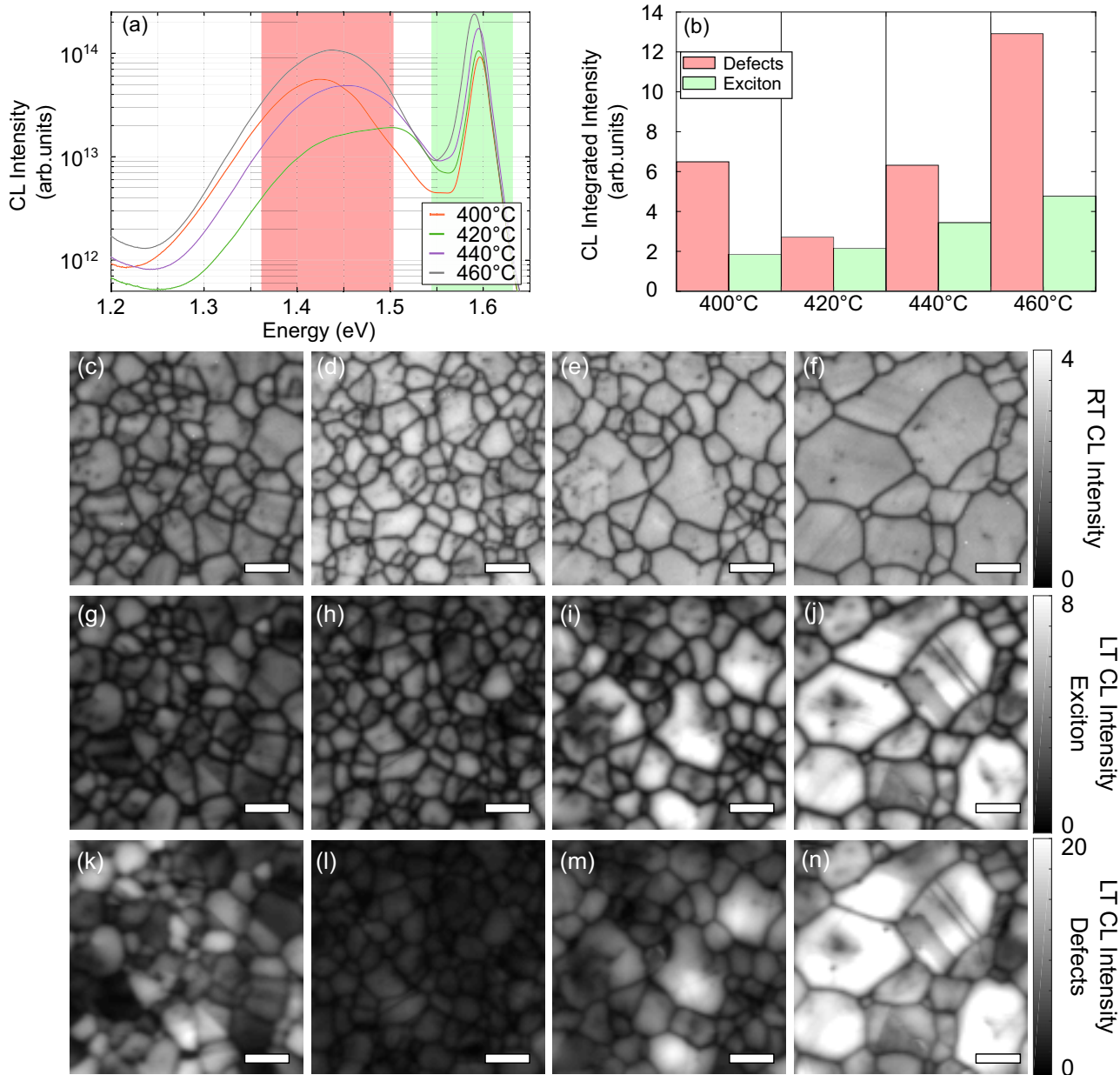


FIG. 5. (a) Low-temperature (10 K) average CL spectra for CdCl₂ samples annealed at different temperatures. Spectra are extracted from LT CL maps (128 × 128 pixels). (b) CL intensity (LT) integrated over [1.361 eV, 1.505 eV] and [1.544 eV, 1.631 eV] for the defect and exciton bands, respectively. The same integrated ranges are used in the CL maps (g)–(n). (c)–(n) CL maps (101 × 101 pixels) measured at room temperature (c)–(f) and low temperature (g)–(n) at the same position for each CdTe sample annealed at CdCl₂ treatment temperature of 400 °C (c),(g),(k); 420 °C (d),(h),(l); 440 °C (e),(i),(m); and 460 °C (f),(j),(n). For LT CL maps, the intensity is integrated on the exciton (f)–(i) or defect (j)–(m) spectral range. Scale bar: 5 μm.

In contrast, the higher annealing temperature is responsible for an increase of the bulk defect density and a decrease of both the GI luminescence and the diffusion length. Hence, the optimal temperature is the result of a tradeoff between GB passivation, grain size, and GI defect density.

Dislocations (line defects) and stacking faults (planar defects) are more visible for the higher annealing temperatures. They are correlated with a lower luminescence, but not with an increase of the A-band emission. The formation and the nature of these structural defects and their detrimental effect on the luminescence are still unclear. Additional characterization

based on transmission electron microscopy (TEM) or electron backscatter diffraction (EBSD) microscopy correlated with CL maps could help in answering these questions.

Postdeposition treatments are important to improve the quality of polycrystalline photovoltaic thin films such as CdTe and Cu(In,Ga)(Se,S)₂. We have shown that RT and LT high-resolution cathodoluminescence maps can be used to correlate the transport and radiative properties to the density of defects. Combining high-resolution CL maps with time-resolved photoluminescence (PL) experiments could provide additional insights into the physics of charge-carrier dynamics in

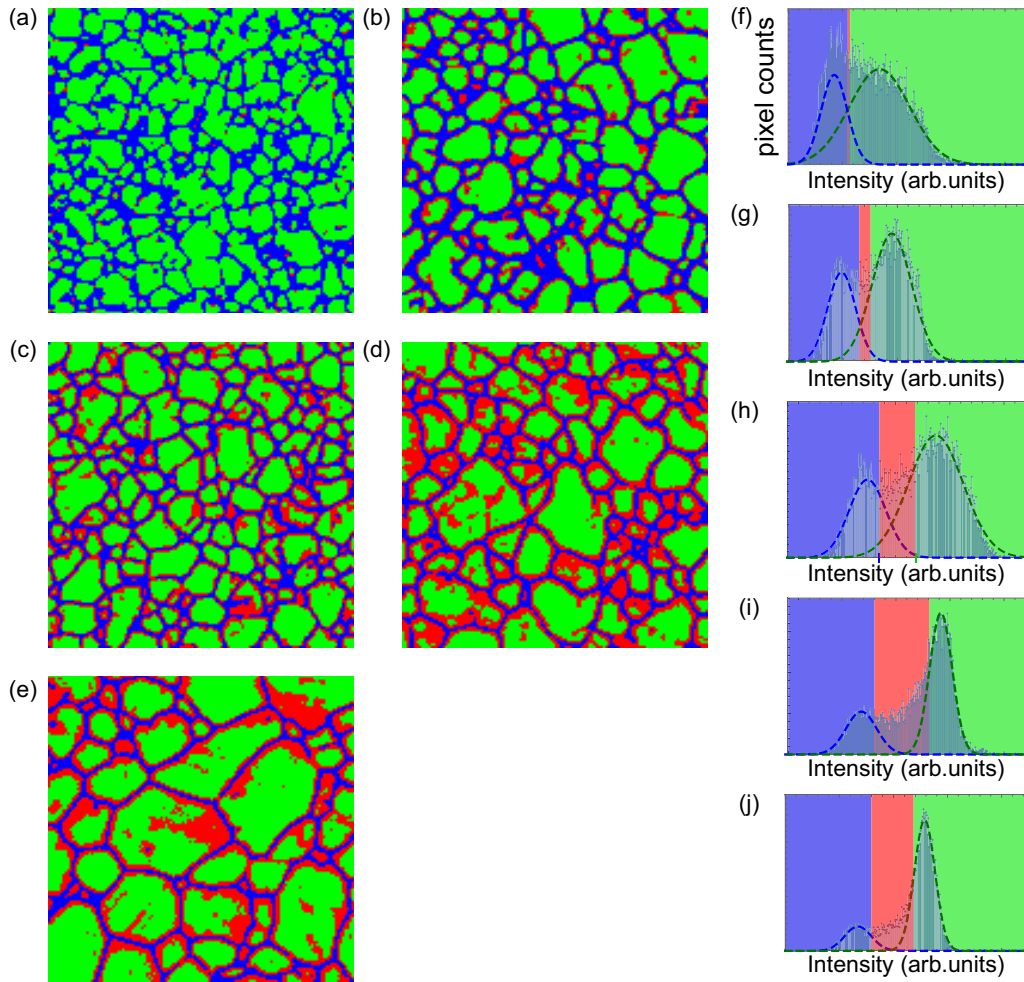


FIG. 6. RT CL maps (a)–(e) and corresponding histograms of the pixel counts as a function of the CL intensity (f)–(j): (a),(f) as-deposited, (b),(g) 400 °C, (c),(h) 420 °C, (d),(i) 440 °C, and (e),(j) 460 °C. Different colors are attributed to the three families: grain boundaries for the low-intensity peak (blue, intensity range $[0; I_{GB} + \sigma_{GB}]$), grain interiors for the high-intensity peak (green, intensity range $[I_{GI} - \sigma_{GI}; \infty]$), and an intermediate family (red, intensity range $[I_{GB} + \sigma_{GB}; I_{GI} - \sigma_{GI}]$). The parameters (I_{GB} , σ_{GB}) and (I_{GI} , σ_{GI}) were fitted with Gaussian functions as described in the text, and given in Table I. The samples and measurement data are identical to Fig. 2.

polycrystalline CdTe thin films. However, linking macroscopic PL measurements with the nanoscopic properties probed by CL remains a challenging task. It requires advanced modeling to account for the complex phenomena occurring in individual grains and the inhomogeneity of thin films.

ACKNOWLEDGMENTS

This work was authored in part by the Alliance for Sustainable Energy, LLC, the manager and operator of the National Renewable Energy Laboratory for the U.S. Department of Energy (DOE) under Contract No. DE-AC36-08GO28308. Funding provided by the US Department of Energy's Office of

Energy Efficiency and Renewable Energy (EERE) under Solar Energy Technologies Office (SETO) Agreement No. 34353. The views expressed in the article do not necessarily represent the views of the DOE or the U.S. Government.

APPENDIX

Figure 6(a)–6(e) shows the RT CL maps plotted in Fig. 1 with colors defined according to the CL intensity for each pixel, as shown in the histograms (f)–(j). It highlights the three different families of pixels: grain interiors in green, grain boundaries in blue, and an intermediate family of defect regions in red, which appears for the higher annealing temperatures.

[1] M. Powalla, S. Paetel, E. Ahlswede, R. Wuerz, C. D. Wessendorf, and T. Magorian Friedlmeier, Thin-film solar cells exceeding 22% solar cell efficiency: An overview on CdTe-, Cu(In,Ga)Se₂-, and perovskite-based materials, *Appl. Phys. Rev.* **5**, 041602 (2018).

[2] A. Kanevce, J. Moseley, M. Al-Jassim, and W. K. Metzger, Quantitative determination of grain-boundary recombination velocity in CdTe by cathodoluminescence measurements and numerical simulations, *IEEE J. Photovoltaics* **5**, 1722 (2015).

- [3] A. Kanevce, M. O. Reese, T. M. Barnes, S. A. Jensen, and W. K. Metzger, The roles of carrier concentration and interface, bulk, and grain-boundary recombination for 25% efficient CdTe solar cells, *J. Appl. Phys.* **121**, 214506 (2017).
- [4] J. M. Burst, J. N. Duenow, D. S. Albin, E. Colegrove, M. O. Reese, J. A. Aguiar, C.-S. Jiang, M. Patel, M. M. Al-Jassim, D. Kuciauskas, S. Swain, T. Ablekim, K. G. Lynn, and W. K. Metzger, CdTe solar cells with open-circuit voltage breaking the 1 V barrier, *Nature Energy* **1**, 16015 (2016).
- [5] J. D. Major, Grain boundaries in CdTe thin film solar cells: A review, *Semicond. Sci. Technol.* **31**, 093001 (2016).
- [6] J. D. Major, M. Al Turkestani, L. Bowen, M. Brossard, C. Li, P. Lagoudakis, S. J. Pennycook, L. J. Phillips, R. E. Treharne, and K. Durose, In-depth analysis of chloride treatments for thin-film CdTe solar cells, *Nat. Commun.* **7**, 13231 (2016).
- [7] K. Akimoto, H. Okuyama, M. Ikeda, and Y. Mori, Oxygen doping in CdTe, CdS and ZnS, *J. Cryst. Growth* **117**, 420 (1992).
- [8] N. Armani, G. Salviati, L. Nasi, A. Bosio, S. Mazzamuto, and N. Romeo, Role of thermal treatment on the luminescence properties of CdTe thin films for photovoltaic applications, *Thin Solid Films* **515**, 6184 (2007).
- [9] V. Consonni and G. Feuillet, Correlated structural reordering and dopant redistribution in annealed polycrystalline CdTe, *J. Appl. Phys.* **105**, 083535 (2009).
- [10] H. Guthrey, J. Moseley, J. Nishinaga, H. Shibata, H. Takahashi, and M. Al-Jassim, Spatially resolved recombination analysis of $\text{CuIn}_x\text{Ga}_{1-x}\text{Se}_2$ absorbers with alkali postdeposition treatments, *IEEE J. Photovoltaics* **8**, 1833 (2018).
- [11] R. Hajimammadov, N. Fathi, A. Bayramov, G. Khrypunov, N. Klochko, and T. Li, Effect of CdCl_2 treatment on properties of CdTe-based solar cells prepared by physical vapor deposition and close-spaced sublimation methods, *Jpn. J. Appl. Phys.* **50**, 05FH01 (2011).
- [12] M. Nakamura, K. Yamaguchi, Y. Kimoto, Y. Yasaki, T. Kato, and H. Sugimoto, Cd-free $\text{Cu}(\text{In,Ga})(\text{Se,S})_2$ thin-film solar cell with record efficiency of 23.35%, *IEEE J. Photovoltaics* **9**, 1863 (2019).
- [13] K. Nakamura, T. Fujihara, T. Toyama, and H. Okamoto, Influence of CdCl_2 treatment on structural and electrical properties of highly efficient 2- μm -thick CdS/CdTe thin film solar cells, *Jpn. J. Appl. Phys.* **41**, 4474 (2002).
- [14] M. M. Nowell, M. A. Scarpulla, N. R. Paudel, K. A. Wieland, A. D. Compaan, and X. Liu, Characterization of sputtered CdTe thin films with electron backscatter diffraction and correlation with device performance, *Microsc. Microanal.* **21**, 927 (2015).
- [15] M. Amarasinghe, E. Colegrove, J. Moseley, H. Moutinho, D. Albin, J. Duenow, S. Jensen, J. Kephart, W. Sampath, S. Sivananthan, M. Al-Jassim, and W. K. Metzger, Obtaining large columnar CdTe grains and long lifetime on nanocrystalline CdSe, MgZnO, or CdS layers, *Adv. Energy Mater.* **8**, 1702666 (2018).
- [16] W. K. Metzger, D. Albin, M. J. Romero, P. Dippo, and M. Young, CdCl_2 treatment, S diffusion, and recombination in polycrystalline CdTe, *J. Appl. Phys.* **99**, 103703 (2006).
- [17] H. R. Moutinho, R. G. Dhere, M. J. Romero, C.-S. Jiang, B. To, and M. M. Al-Jassim, Electron backscatter diffraction of CdTe thin films: Effects of CdCl_2 treatment, *J. Vac. Sci. Technol. A* **26**, 1068 (2008).
- [18] J. Mendoza-Alvarez, J. González-Hernández, F. Sánchez-Sinencio, O. Zelaya, and S. Chao, Luminescence and particle size in microcrystalline CdTe thin films, *J. Cryst. Growth* **86**, 391 (1988).
- [19] J. Lee, Effects of heat treatment of vacuum evaporated CdCl_2 layer on the properties of CdS/CdTe solar cells, *Curr. Appl. Phys.* **11**, S103 (2011).
- [20] J. Moseley, P. Rale, S. Collin, E. Colegrove, H. Guthrey, D. Kuciauskas, H. Moutinho, M. Al-Jassim, and W. K. Metzger, Luminescence methodology to determine grain-boundary, grain-interior, and surface recombination in thin-film solar cells, *J. Appl. Phys.* **124**, 113104 (2018).
- [21] C. Jiang, H. Moutinho, J. Moseley, A. Kanevce, J. Duenow, E. Colegrove, C. Xiao, W. Metzger, and M. Al-Jassim, Simultaneous examination of grain-boundary potential, recombination, and photocurrent in CdTe solar cells using diverse nanometer-scale imaging, in *2017 IEEE 44th Photovoltaic Specialist Conference (PVSC)* (IEEE, Washington, DC, 2017), pp. 1312–1316.
- [22] J. D. Poplawsky, N. R. Paudel, C. Li, C. M. Parish, D. Leonard, Y. Yan, and S. J. Pennycook, Direct imaging of Cl- and Cu-induced short-circuit efficiency changes in CdTe solar cells, *Adv. Energy Mater.* **4**, 1400454 (2014).
- [23] J. D. Poplawsky, C. Li, N. R. Paudel, W. Guo, Y. Yan, and S. J. Pennycook, Nanoscale doping profiles within CdTe grain boundaries and at the CdS/CdTe interface revealed by atom probe tomography and STEM EBIC, *Sol. Energy Mater. Sol. Cells* **150**, 95 (2016).
- [24] S. Galloway, P. Edwards, and K. Durose, Characterisation of thin film CdS/CdTe solar cells using electron and optical beam induced current, *Sol. Energy Mater. Sol. Cells* **57**, 61 (1999).
- [25] R. Cohen, V. Lyahovitskaya, E. Poles, A. Liu, and Y. Rosenwaks, Unusually low surface recombination and long bulk lifetime in *n*-CdTe single crystals, *Appl. Phys. Lett.* **73**, 1400 (1998).
- [26] W. K. Metzger and M. Gloeckler, The impact of charged grain boundaries on thin-film solar cells and characterization, *J. Appl. Phys.* **98**, 063701 (2005).
- [27] S. A. Jensen, J. M. Burst, J. N. Duenow, H. L. Guthrey, J. Moseley, H. R. Moutinho, S. W. Johnston, A. Kanevce, M. M. Al-Jassim, and W. K. Metzger, Long carrier lifetimes in large-grain polycrystalline CdTe without CdCl_2 , *Appl. Phys. Lett.* **108**, 263903 (2016).
- [28] J. M. Burst, J. N. Duenow, A. Kanevce, H. R. Moutinho, C. S. Jiang, M. M. Al-Jassim, M. O. Reese, D. S. Albin, J. A. Aguiar, E. Colegrove, T. Ablekim, S. K. Swain, K. G. Lynn, D. Kuciauskas, T. M. Barnes, and W. K. Metzger, Interface characterization of single-crystal CdTe solar cells with 950 mV, *IEEE J. Photovoltaics* **6**, 1650 (2016).
- [29] D. Kuciauskas, P. Dippo, A. Kanevce, Z. Zhao, L. Cheng, A. Los, M. Gloeckler, and W. K. Metzger, The impact of Cu on recombination in high voltage CdTe solar cells, *Appl. Phys. Lett.* **107**, 243906 (2015).
- [30] W. K. Metzger, S. Grover, D. Lu, E. Colegrove, J. Moseley, C. L. Perkins, X. Li, R. Mallick, W. Zhang, R. Malik, J. Kephart, C.-S. Jiang, D. Kuciauskas, D. S. Albin, M. M. Al-Jassim, G. Xiong, and M. Gloeckler, Exceeding 20% efficiency with in situ group V doping in polycrystalline CdTe solar cells, *Nature Energy* **4**, 837 (2019).
- [31] E. Regalado-Pérez, M. G. Reyes-Banda, and X. Mathew, Influence of oxygen concentration in the CdCl_2 treatment process

- on the photovoltaic properties of CdTe/CdS solar cells, *Thin Solid Films* **582**, 134 (2015).
- [32] M. Amarasinghe, S. Sivananthan, W. K. Metzger, E. Colegrove, H. Moutinho, D. Albin, J. Duenow, S. Johnston, J. Kephart, W. Sampath, and M. Al-Jassim, Influence of CdTe deposition temperature and window thickness on CdTe grain size and lifetime after CdCl₂ recrystallization, *IEEE J. Photovoltaics* **8**, 600 (2018).
- [33] T. A. M. Fiducia, B. G. Mendis, K. Li, C. R. M. Grovenor, A. H. Munshi, K. Barth, W. S. Sampath, L. D. Wright, A. Abbas, J. W. Bowers, and J. M. Walls, Understanding the role of selenium in defect passivation for highly efficient selenium-alloyed cadmium telluride solar cells, *Nature Energy* **4**, 504 (2019).
- [34] E. S. Barnard, B. Ursprung, E. Colegrove, H. R. Moutinho, N. J. Borys, B. E. Hardin, C. H. Peters, W. K. Metzger, and P. J. Schuck, 3D lifetime tomography reveals how CdCl₂ improves recombination throughout CdTe solar cells, *Adv. Mater.* **29**, 1603801 (2017).
- [35] H. R. Moutinho, J. Moseley, M. J. Romero, R. G. Dhere, C.-S. Jiang, K. M. Jones, J. N. Duenow, Y. Yan, and M. M. Al-Jassim, Grain boundary character and recombination properties in CdTe thin films, in *2013 IEEE 39th Photovoltaic Specialists Conference (PVSC)* (IEEE, Tampa, FL, 2013), pp. 3249–3254.
- [36] L. Zhang, J. L. F. Da Silva, J. Li, Y. Yan, T. A. Gessert, and S.-H. Wei, Effect of Copassivation of Cl and Cu on CdTe Grain Boundaries, *Phys. Rev. Lett.* **101**, 155501 (2008).
- [37] J. Moseley, W. K. Metzger, H. R. Moutinho, N. Paudel, H. L. Guthrey, Y. Yan, R. K. Ahrenkiel, and M. M. Al-Jassim, Recombination by grain-boundary type in CdTe, *J. Appl. Phys.* **118**, 025702 (2015).
- [38] S. P. Harvey, G. Teeter, H. Moutinho, and M. M. Al-Jassim, Direct evidence of enhanced chlorine segregation at grain boundaries in polycrystalline CdTe thin films via three-dimensional TOF-SIMS imaging, *Prog. Photo.: Res. Appl.* **23**, 838 (2014).
- [39] D. Mao, G. Blatz, C. Wickersham Jr., and M. Gloeckler, Correlative impurity distribution analysis in cadmium telluride (CdTe) thin-film solar cells by ToF-SIMS 2D imaging, *Sol. Energy Mater. Sol. Cells*, **157**, 65 (2016).
- [40] C. Li, Y. Wu, J. Poplawsky, T. J. Pennycook, N. Paudel, W. Yin, S. J. Haigh, M. P. Oxley, A. R. Lupini, M. Al-Jassim, S. J. Pennycook, and Y. Yan, Grain-Boundary-Enhanced Carrier Collection in CdTe Solar Cells, *Phys. Rev. Lett.* **112**, 156103 (2014).
- [41] T. A. M. Fiducia, K. Li, A. H. Munshi, K. Barth, W. S. Sampath, C. R. M. Grovenor, and J. M. Walls, 3D distributions of chlorine and sulphur impurities in a thin-film cadmium telluride solar cell, *MRS Adv.* **3**, 3287 (2018).
- [42] D. M. Hofmann, P. Omling, H. G. Grimmeiss, B. K. Meyer, K. W. Benz, and D. Sinerius, Identification of the chlorine A center in CdTe, *Phys. Rev. B* **45**, 6247 (1992).
- [43] J. Moseley, M. M. Al-Jassim, H. R. Moutinho, H. L. Guthrey, W. K. Metzger, and R. K. Ahrenkiel, Explanation of red spectral shifts at CdTe grain boundaries, *Appl. Phys. Lett.* **103**, 233103 (2013).
- [44] W. Van Roosbroeck, Injected current carrier transport in a semi-infinite semiconductor and the determination of lifetimes and surface recombination velocities, *J. Appl. Phys.* **26**, 380 (1955).
- [45] B. G. Mendis, L. Bowen, and Q. Z. Jiang, A contactless method for measuring the recombination velocity of an individual grain boundary in thin-film photovoltaics, *Appl. Phys. Lett.* **97**, 092112 (2010).
- [46] B. G. Mendis, D. Gachet, J. D. Major, and K. Durose, Long Lifetime Hole Traps at Grain Boundaries in CdTe Thin-Film Photovoltaics, *Phys. Rev. Lett.* **115**, 218701 (2015).
- [47] D. Halliday, J. Eggleston, and K. Durose, A photoluminescence study of polycrystalline thin-film CdTe/CdS solar cells, *J. Cryst. Growth* **186**, 543 (1998).
- [48] C. Kraft, H. Metzner, M. Hädrich, U. Reislöhner, P. Schley, G. Gobsch, and R. Goldhahn, Comprehensive photoluminescence study of chlorine activated polycrystalline cadmium telluride layers, *J. Appl. Phys.* **108**, 124503 (2010).